Turk J Elec Engin, VOL.16, NO.1 2008, © TÜBİTAK

Recent Advances in Perfectly Matched Layers in Finite Element Applications

Özlem ÖZGÜN and Mustafa KUZUOĞLU
Department of Electrical and Electronics Engineering, Middle East Technical University
06531, Ankara-TURKEY

Abstract

We present a comparative evaluation of two novel and practical perfectly matched layer (PML) implementations to the problem of mesh truncation in the finite element method (FEM): locally-conformal PML, and multi-center PML techniques. The most distinguished feature of these methods is the simplicity and flexibility to design conformal PMLs over challenging geometries, especially those with curvature discontinuities, in a straightforward way without using artificial absorbers. These methods are based on specially- and locally-defined complex coordinate transformations inside the PML region. They can easily be implemented in a conventional FEM by just replacing the nodal coordinates inside the PML region by their complex counterparts obtained via complex coordinate transformation. After overviewing the theoretical bases of these methods, we present some numerical results in the context of two- and three-dimensional electromagnetic radiation/scattering problems.

Key Words: *Finite element method (FEM); perfectly matched layer (PML); locally-conformal PML; multi-center PML; complex coordinate stretching; electromagnetic scattering.*

1. Introduction

Perfectly matched layers (PMLs) have been popular in the finite element method (FEM) and the finite difference time domain method (FDTD) for solving the domain truncation problem in electromagnetic radiation and scattering problems. The PML approach is based on the truncation of computational domain by a reflectionless artificial layer which absorbs outgoing waves regardless of their frequency and angle of incidence. The main advantage of the PML is its close proximity and conformity to the surface of the radiator or scatterer, implying that the white space can be minimized.

The PML concept has been introduced by Berenger [1] in the FDTD method by using a split-field formulation in cartesian coordinates. Alternatively, Chew and Weedon [2] achieved a PML action in the FDTD via the concept of complex coordinate stretching, which is basically the analytic continuation of the electromagnetic fields to complex space. Both approaches yield non-Maxwellian fields within the PML domain. A touchstone to initiate the implementation of the PML in the FEM is achieved by Sacks et al. [3], who constructed a Maxwellian PML in cartesian coordinates as an 'anisotropic layer' with appropriately defined permittivity and permeability tensors. The anisotropic PML has been extended to cylindrical and spherical coordinates [4], and has been used in the design of conformal PMLs using a local curvilinear

coordinate system [5]. Then, the anisotropic PML has been investigated extensively in literature [6–11]. The concept of coordinate stretching has also been used in the FEM, not directly, but through the mapping of the non-Maxwellian fields obtained during the complex coordinate transformation to a set of Maxwellian fields in an anisotropic medium representing the PML [12].

All of the above-mentioned PML approaches in the FEM history employ artificial absorbing materials and a local/nonlocal coordinate system in order to design the PML as an 'anisotropic medium' having suitably defined constitutive parameters. In addition, a majority of PML realizations in FEM simulations have been implemented in a rectangular prism or spherical PML domain, which does not have arbitrary curvature discontinuities. However, the *locally-conformal PML* [13–16] and *multi-center PML* [16, 17] methods are non-Maxwellian PML implementations which do not use any artificial anisotropic materials and coordinate system. These methods utilize a specially- and locally-defined complex coordinate stretching, and thus, make possible the easy design of conformal PMLs having challenging geometries, especially having some intersection regions or abrupt changes in curvature. Such conformal PML domains are very crucial especially in radiation and scattering problems, because they decrease the computational demand (such as memory and processing power) on account of a minimization of the white space. The locally-conformal PML and multi-center PML methods are designed in complex space by just replacing the real coordinates with their complex counterparts calculated in terms of the complex coordinate transformation. This is due to the fact that the equations related to the FEM formulation in the PML region are expressed directly by the nodal coordinates. In this formulation, Maxwell's equations are modified accordingly inside the complex space, and the elements in the real coordinate system are mapped to the *complex elements* (i.e., elements whose nodal coordinates are complex) in complex space. Then, the weak variational form of the wave equation is discretized using these complex elements which are determined by the complex coordinate transformation.

In this paper, we first overview the equations governing the parametric construction of the locally-conformal PML and multi-center PML methods in Sections 2 and 3, respectively. Then, we demonstrate some numerical applications involving electromagnetic radiation/scattering problems in Section 4.

2. Locally-Conformal PML Method

In both locally-conformal PML and multi-center PML methods, the initial step is the spatial construction of the PML region (Ω_{PML}) as conformal to an arbitrary source volume Ω containing sources and objects (or scatterers). The source volume can be determined as the convex hull (i.e., the smallest convex set that encloses the sources and objects) to minimize the computational domain. We illustrate the locally-conformal PML method in Figure 1(a), which shows a partial cross-section of an arbitrary PML region Ω_{PML} enclosed within the boundaries $\partial\Omega_a$ and $\partial\Omega_b$.

In the locally-conformal PML method, each point P in Ω_{PML} is mapped to $\tilde{P}$ in complex PML region $\Gamma \subset C^3$, through the complex coordinate transformation which is defined as (assuming a suppressed time-dependence $e^{j\omega t}$)

$$\tilde{\vec{r}} = \vec{r} + \frac{1}{jk} f(\xi)\, \hat{n}(\xi) \tag{1}$$

where $\vec{r} \in \Re^3$ and $\tilde{\vec{r}} \in C^3$ are the position vectors of the points P in real space and $\tilde{P}$ in complex space, respectively; k represents the wave number; and ξ is the parameter defined by

$$\xi = \|\vec{r} - \vec{r}_a\|, \tag{2}$$

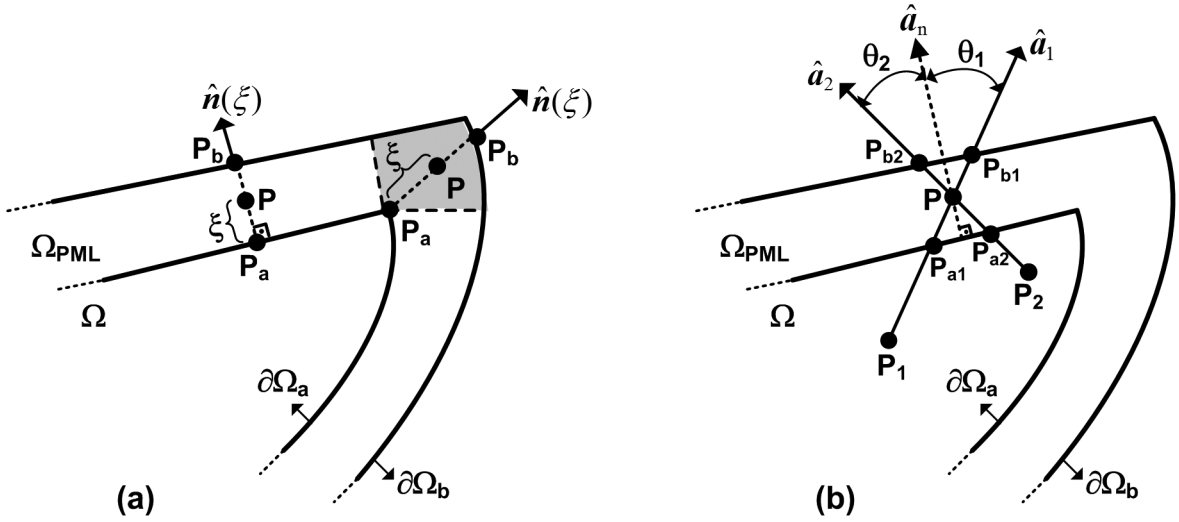

Figure 1. (a) Locally-conformal PML, (b) Multi-center PML.

where $\vec{r}_a \in \partial\Omega_a$ is the position vector of the point P_a located on $\partial\Omega_a$, which is the solution of the minimization problem

$$\min_{\vec{r}_a \in \partial\Omega_a} \|\vec{r} - \vec{r}_a\| . \tag{3}$$

Equation (3) yields a unique $\vec{r}_a$ because $\partial\Omega_a$ is the boundary of the convex set, and which can be simply performed by using some search techniques in the mesh coordinates of the conventional FEM program. Furthermore, $\hat{n}(\xi)$ is the unit vector defined by

$$\hat{n}(\xi) = (\vec{r} - \vec{r}_a)/\xi \tag{4}$$

and $f(\xi)$ is a monotonically increasing function of ξ as follows

$$f(\xi) = \frac{\alpha\, \xi^m}{m\, \|\vec{r}_b - \vec{r}_a\|^{m-1}}, \tag{5}$$

where α is a positive parameter (practically, $5k \leq \alpha \leq 15k$ for a PML thickness between $\lambda/4$ and $\lambda/2$ where λ is the wavelength), m is a positive integer (typically 2 or 3) related to the decay rate of the magnitude of the field inside Ω_{PML}, and $\vec{r}_b$ is the position vector of the point P_b which is the intersection of the line passing through $\vec{r}$ and $\vec{r}_b$ (i.e., the dotted line in Figure 1(a)) and $\partial\Omega_b$. We note that $\|\vec{r}_b - \vec{r}_a\|$ represents the local PML thickness for the corresponding PML point. The transformation in (1) can be implemented in a FEM program by replacing the real-valued node coordinates inside Ω_{PML} by their complex-valued counterparts calculated by (1).

It is worth mentioning that the transformation in (1) is *local*, meaning that each PML point has its own parameters depending on its position inside the PML region. Therefore, the geometry of $\partial\Omega_a$ is not important, and the transformation yields analytic continuity even in the case of curvature discontinuities on $\partial\Omega_a$. It is evident that if the curvature of $\partial\Omega_a$ is continuous, the unit vector is normal to $\partial\Omega_a$. In addition, the transformation in (1) meets the following three conditions which are essential for a successful PML design:

(i) the outgoing wave in the neighborhood of P_a is transmitted into Ω_{PML} without any reflection;

(ii) the transmitted wave decays monotonically within Ω_{PML} along the direction of the unit vector;

(iii) the magnitude of the transmitted wave is negligible on $\partial\Omega_b$.

Inside the complex PML space, the Maxwell's equations are modified as follows

$$\tilde{\nabla} \times \vec{E}^c\left(\tilde{\vec{r}}\right) = -j\omega\mu_0 \vec{H}^c\left(\tilde{\vec{r}}\right) \tag{6a}$$

$$\tilde{\nabla} \times \vec{H}^c\left(\tilde{\vec{r}}\right) = j\omega\varepsilon_0 \vec{E}^c\left(\tilde{\vec{r}}\right), \tag{6b}$$

where ε_0 and μ_0 are free-space permittivity and permeability values, respectively; $\vec{E}^c\left(\tilde{\vec{r}}\right)$ and $\vec{H}^c\left(\tilde{\vec{r}}\right)$ are the analytic continuation of $\vec{E}\left(\vec{r}\right)$ and $\vec{H}\left(\vec{r}\right)$ to complex space, respectively; and $\tilde{\nabla}$ is the nabla operator in complex space and is given by

$$\tilde{\nabla} = [\bar{\bar{J}}^{-1}]^T \cdot \nabla, \tag{7}$$

where $\bar{\bar{J}} = \partial\left(\tilde{x}, \tilde{y}, \tilde{z}\right)/\partial\left(x, y, z\right)$ is the Jacobian tensor. Then, the vector wave equation in complex space is derived as

$$\tilde{\nabla} \times \tilde{\nabla} \times \vec{E}^c\left(\tilde{\vec{r}}\right) - k^2 \vec{E}^c\left(\tilde{\vec{r}}\right) = 0. \tag{8}$$

Using the method of weighted residuals, the weak form of this wave equation is expressed as

$$\int\limits_{\Omega_{PML}} \left[\tilde{\nabla} \times \vec{E}^c\left(\tilde{\vec{r}}\right)\right] \cdot \left[\tilde{\nabla} \times \vec{W}^c\right] d\Omega - k^2 \int\limits_{\Omega_{PML}} \vec{E}^c\left(\tilde{\vec{r}}\right) \cdot \vec{W}^c d\Omega = 0, \tag{9}$$

where $\vec{W}^c$ is a vector weight function in complex space. In the FEM, we solve (9) by discretizing the computational domain using *complex* edge elements (such as tetrahedrons). It is obvious that the equations governing the FEM formulation preserve their form inside the PML region, except that the coordinate variables are complex. Similarly, in 2D, the Helmholtz equation preserves its form in complex space. Then, the weak form of the Helmhotz equation in complex space is solved by discretizing the computational domain using *complex* nodal elements (such as triangles). Although the fields $\vec{E}^c\left(\tilde{\vec{r}}\right)$ and $\vec{H}^c\left(\tilde{\vec{r}}\right)$ in the complex PML region are non-Maxwellian in terms of the real coordinate variables, the FEM formulation can still be carried out within the PML region which is a subset of the complex space (it is shown in [13, 14] in detail). If a Maxwellian PML is desired, the locally-conformal PML may also be extended to obtain an anisotropic PML by mapping the resulting non-Maxwellian fields to Maxwellian fields in an anisotropic medium, as shown in [14]. However, this anisotropic PML implementation is much more complicated both analytically and computationally.

3. Multi-Center PML Method

The multi-center PML method, which is illustrated in Figure 1(b), is basically a generalization of the locally-conformal PML method. This method is based on a finite number of center points (such as P_1 and P_2 in Figure 1(b)) inside the source volume (Ω). After choosing the centers appropriately, the unit vectors ($\hat{a}_1$

and $\hat{a}_2$) corresponding to each center point are calculated emanating from these centers in the direction of the PML point, P. Then, the points on the boundaries $\partial\Omega_a$ and $\partial\Omega_b$ (i.e., P_{a1}, P_{b1}, P_{a2} and P_{b2}) are determined using these unit vectors, as shown in Figure 1(b). The unit vector $\hat{a}_n$, which is shown by the dotted line, is equivalent to $\hat{n}(\xi)$ in (4). Moreover, θ_1 and θ_2 are the angles between $\hat{a}_n$ and the unit vectors $\hat{a}_1$ and $\hat{a}_2$, respectively.

In the multi-center PML method, the complex coordinate transformation which maps each point P in Ω_{PML} to $\tilde{P}$ in complex PML region $\Gamma \subset C^3$, is defined as follows

$$\vec{r}' = \vec{r} + \frac{\alpha}{jk} \sum_{i=1}^{N} w_i \frac{(d_{ai})^m}{m\,(d_{bi})^{m-1}} \hat{a}_i, \tag{10}$$

where α and m are the same as before, N is the number of the centers, d_{ai} is the distance between P and P_{ai} for the i-th center (P_i), d_{bi} is the distance between P_{bi} and P_{ai} for P_i, and w_i is the real weight value assigned to P_i. The sum of all weights should add up to 1, and each weight w_i is inversely proportional to the angle θ_i, whose value is less than or equal to 45°. The value "45°" is the threshold value in the assignment of the weights, and it has been determined empirically via some numerical experiments [17]. The weight selection scheme assigns the highest priority to the center whose unit vector $\hat{a}_i$ makes the smallest angle with $\hat{a}_n$. In order to achieve smooth decay inside the PML region, the centers should be chosen in such a way that each PML point should have *at least one center*, whose angle θ_i is less than or equal to 45°. In some smooth geometries (such as a spherical or cubical shell), a single center-of-mass point can provide reliable results. The center selection scheme is a straightforward task depending on the geometrical structure of the PML region. It is worth mentioning that the increase in the number of centers creates negligible burden on the memory requirement and the processing power of the computer (compared to those needed for the matrix construction and solution phases of the FEM), because the multi-center PML method is implemented in the pre-processing phase.

Similar to the locally-conformal PML method, the effect of the complex coordinate stretching in (10) can be easily incorporated into the FEM by interchanging the real coordinates with the complex coordinates, because the local FEM matrix entries depend on the coordinate variations.

4. Numerical Examples

In this section, we demonstrate some numerical experiments by means of some two- and three-dimensional (2D and 3D) electromagnetic radiation/scattering problems. In 3D, we consider the problem of scattering by a perfectly-conducting object. In 2D, we consider two problems: (i) TM_z electromagnetic scattering problem involving a single infinitely-long cylindrical perfectly-conducting object with an arbitrary cross-section, and (ii) radiation of a single line-source inside an infinitely-long cylindrical region of arbitrary shape.

While simulating the radiation problem, we take the position of the line-source as a 'random variable' uniformly distributed inside a region because the source position may affect the accuracy. For this purpose, we resort to the "Monte Carlo" simulation technique in order to show that the PML methods achieve reliable and robust results irrespective of the source position. We determine randomly '2000 different source positions', and we run the program 2000 times using them. For each run, we calculate a mean-square error

criterion in Ω as

$$E = \frac{\sum\limits_{\Omega} \left| \vec{E} - \vec{E}^{analytic} \right|^2}{\sum\limits_{\Omega} \left| \vec{E}^{analytic} \right|^2}, \tag{11}$$

where $\vec{E}$ is the field calculated by either the locally-conformal PML method or the multi-center PML method, and $\vec{E}^{analytic}$ is the field calculated analytically in Ω (free-space).

In scattering problems, the performances of the PML methods are tested in terms of the radar-cross-section (RCS) calculations of the objects, and are validated with the results of a standard method-of-moments (MoM) code or literature. The common parameters in all experiments are: k is 20π (i.e., the wavelength λ is 0.1 meter), m is 3, and α is chosen in the range between $5k$–$10k$. In addition, the PML thickness is approximately set to $\lambda/4$.

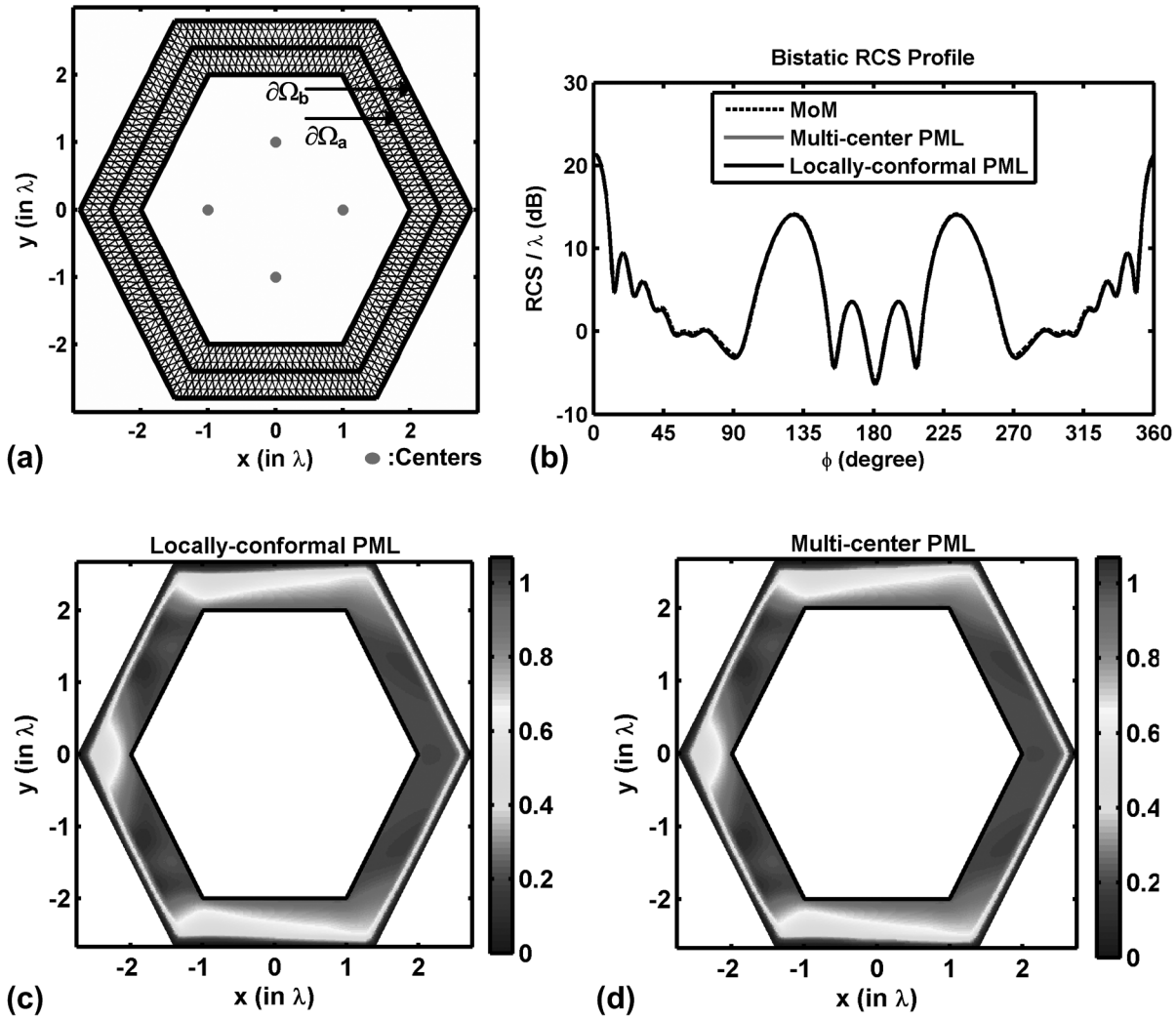

Figure 2. Scattering from a hexagonal cylinder: (a) Mesh structure, (b) RCS profile, (c) Scattered field contour in the locally-conformal PML, (d) Scattered field contour in the multi-center PML.

4.1. 2D Simulations

The first example considers the problem of scattering from a hexagonal cylinder, whose mesh structure with triangular elements is shown in Figure 2(a). Gray dots in this figure indicate the center positions chosen in the multi-center PML implementation. Assuming that the angle of incidence of the plane wave is 180° with respect to the x-axis, we plot the bistatic RCS profiles in Figure 2(b). We also plot the contours of the scattered field (magnitude) for the locally-conformal PML and the multi-center-PML implementations in Figure 2(c) and (d), respectively.

The second example is the problem of radiation by a line-source inside the infinitely-long cylindrical region of 'ogive' cross-section, as shown in Figure 3(a). Five centers are selected in the multi-center PML

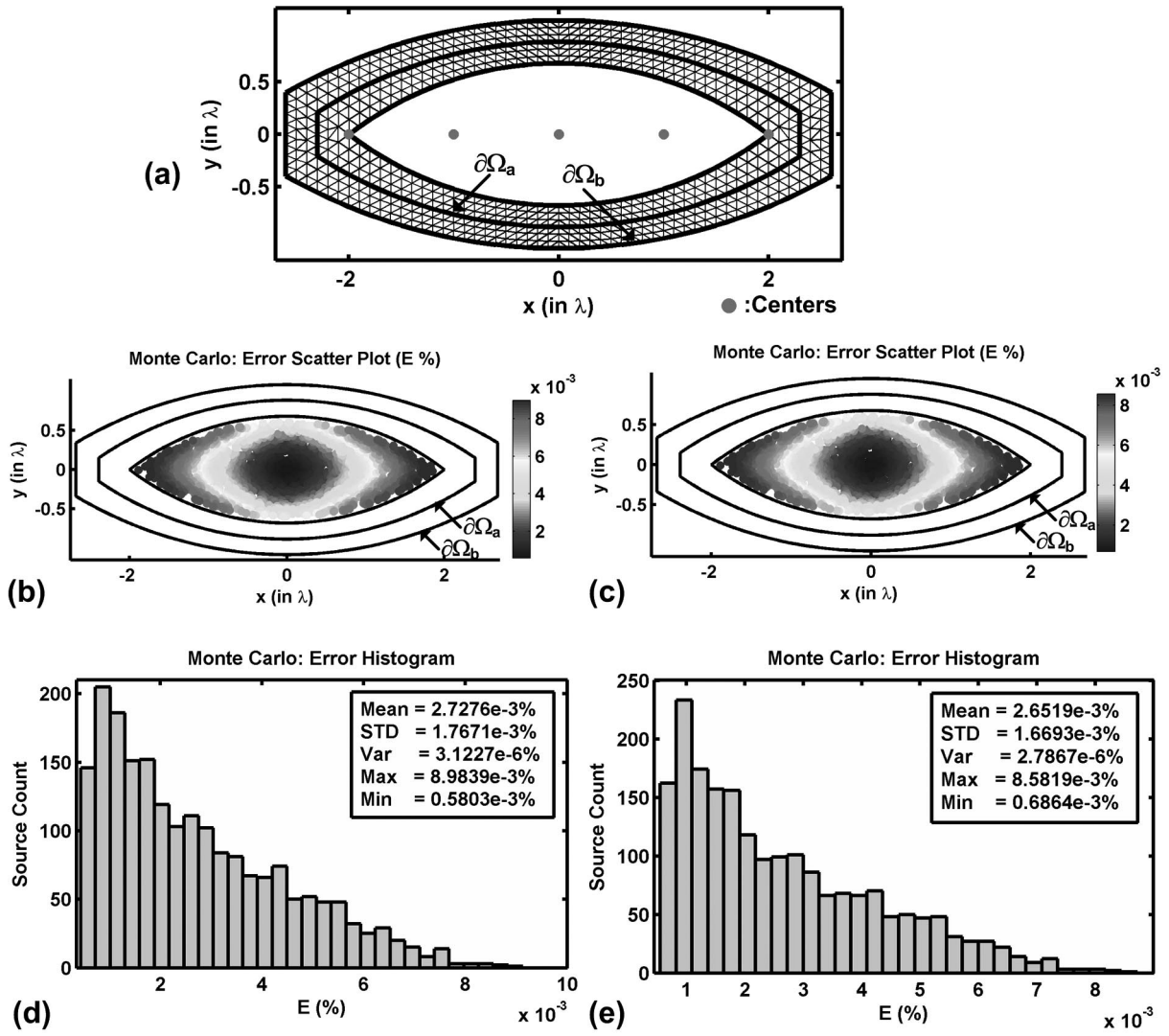

Figure 3. Monte Carlo simulation of the radiation problem in ogive domain: (a) Mesh structure, (b) Error scatter plot in the locally-conformal PML, (c) Error scatter plot in the multi-center PML, (d) Error histogram and statistics in the locally-conformal PML, (e) Error histogram and statistics in the multi-center PML.

implementation. In the Monte Carlo simulation, we choose 2000 different source positions inside the empty (or white) region in Figure 3(a). After we calculate the error values for each run, we plot the error scatter plot (it shows the error value at each source position) in Figure 3(b) and (c) for the locally-conformal PML and multi-center PML methods, respectively. We also plot the error histogram in Figure 3(d) and (e) for the locally-conformal PML and multi-center PML methods, respectively. We show some statistical error values (i.e., mean, variance, etc.) on these plots.

4.2. 3D Simulations

The first problem considers the scattering from a perfectly-conducting cube whose edge length is 0.755λ. The cross-sectional mesh structure using tetrahedral elements is shown in Figure 4(a). The incident plane wave propagates along the positive z-direction, and the electric field is polarized along the y-direction. A single center is chosen at the center-of-mass in the multi-center PML method. We plot the bistatic RCS profiles in Figure 5, by comparing them with [18].

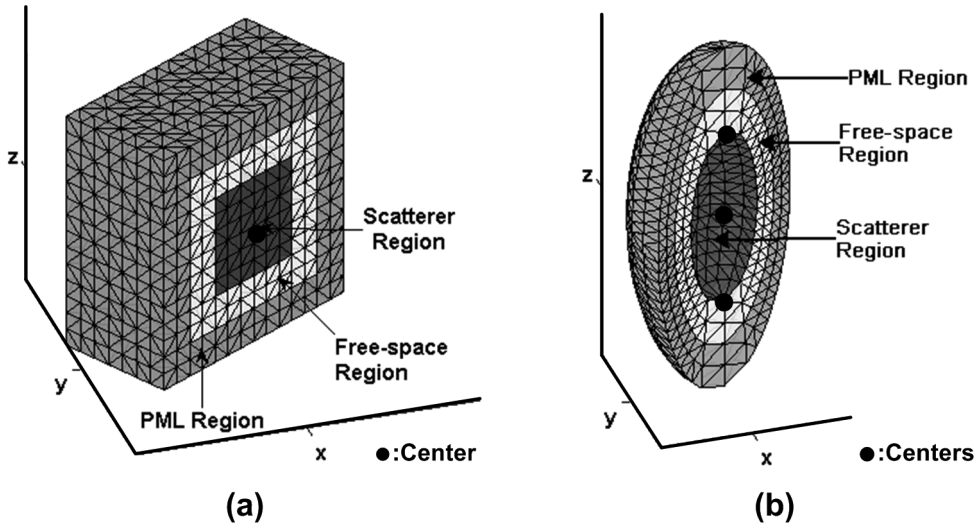

Figure 4. Mesh structure in 3D scattering problem: (a) Cube, (b) Prolate spheroid.

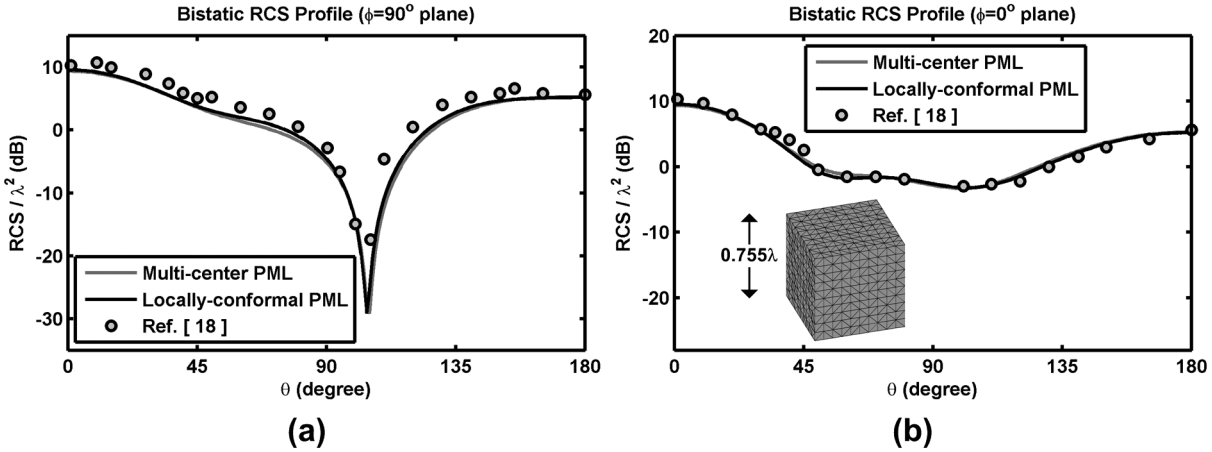

Figure 5. Bistatic RCS profile of cube: (a) $\phi = 90^\circ$ plane, (b) $\phi = 0^\circ$ plane.

The second example deals with scattering from a prolate spheroid whose semi-major axis is 0.8λ and axial ratio is 2. The incident plane wave propagates along the negative z-direction, and the electric field is polarized along the y-direction. Three centers are chosen for the multi-center PML method, as illustrated in Figure 4(b). We plot the bistatic RCS profiles in Figure 6, by comparing them with [19].

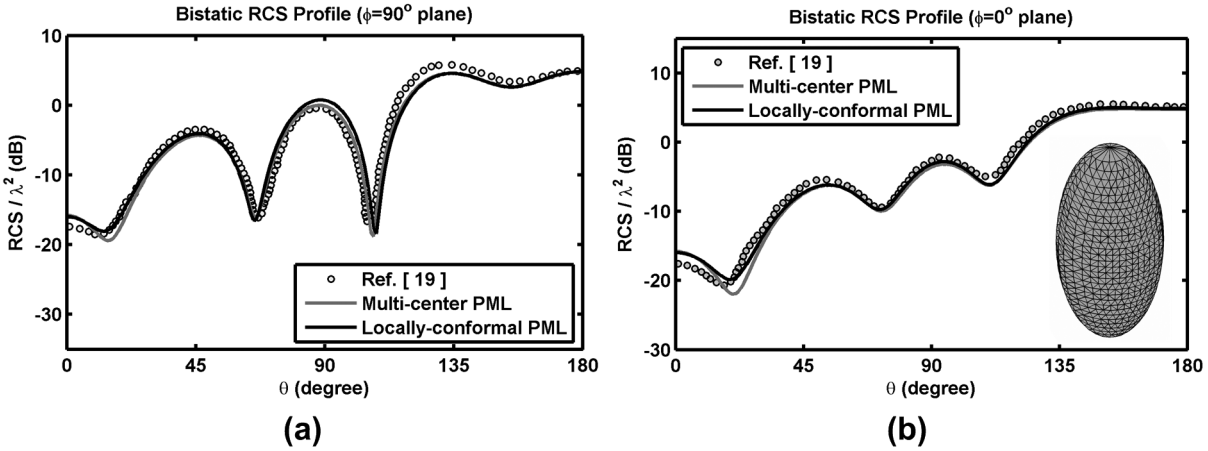

Figure 6. Bistatic RCS profile of prolate spheroid: (a) $\phi = 90^\circ$ plane, (b) $\phi = 0^\circ$ plane.

These examples demonstrate that the locally-conformal PML and the multi-center PML methods are efficient absorbers for the FEM mesh truncation having arbitrary geometries.

5. Conclusion

In this paper, we have presented a comparative evaluation of the locally-conformal PML and multi-center PML methods for finite element mesh truncation. We have shown that these methods are very simple and practical, and they make easier the design of conformal PMLs enclosing arbitrarily-shaped convex sets. The implementations of these methods are based on a single algorithm performing the task which replaces the real coordinates inside the PML region with their complex counterparts calculated by the complex coordinate transformation, without altering the original FEM formulation. We have investigated the accuracy of these methods by means of some numerical comparisons.

References

[1] J.P. Berenger, "A perfectly matched layer for the absorption of electromagnetic waves," J. Comput. Phys., Vol. 114, pp. 185–200, 1994.

[2] W.C. Chew, W. Weedon, "A 3D perfectly matched medium from modified Maxwell's equations with stretched coordinates," Microwave Opt. Technol. Lett., Vol. 7, pp. 599–604, 1994.

[3] Z.S. Sacks, D.M. Kingsland, R. Lee, J.F. Lee, "A perfectly matched anisotropic absorber for use as an absorbing boundary condition," IEEE Trans. Antennas Propagat., Vol. 43, pp. 1460–1463, 1995.

[4] M. Kuzuoglu, R. Mittra, "Investigation of nonplanar perfectly matched absorbers for finite element mesh truncation," IEEE Trans. Antennas Propagat., Vol. 45, pp. 474–486, 1997.

[5] M. Kuzuoglu, R. Mittra, "Mesh truncation by perfectly matched anisotropic absorbers in the finite element method," Microwave Opt. Technol. Lett., Vol. 12, pp. 136–140, 1996.

[6] S.D. Gedney, "An anisotropic perfectly matched layer absorbing medium for the truncation of FDTD lattices," IEEE Trans. Antennas Propagat., Vol. 44, pp. 1630–1639, 1996.

[7] M. Kuzuoglu, R. Mittra, "Frequency dependence of the constitutive parameters of causal perfectly matched anisotropic absorbers," IEEE Microwave Guided Wave Lett., Vol. 6, pp. 447–449, 1996.

[8] J.Y. Wu, D.M. Kingsland, J.F. Lee, R. Lee, "A comparison of anisotropic PML to Berenger's PML and its application to the finite-element method for EM scattering," IEEE Trans. Antennas Propagat., Vol. 45, pp. 40-50, 1997.

[9] M. Kuzuoglu, R. Mittra, "A systematic approach to the derivation of constitutive parameters of a perfectly matched absorber," IEEE Microwave Guided Wave Lett., Vol. 8, no. 9, pp. 313–315, 1998.

[10] M.S. Tong, Y.C. Chen, M. Kuzuoglu, R. Mittra, "A new anisotropic perfectly matched layer medium for mesh truncation in finite difference time domain analysis," Inter. Jour. of Electronics, Vol. 86, no. 9, pp. 1085–1091, 1999.

[11] M. Kuzuoglu, R. Mittra, "A systematic study of perfectly matched absorbers," (in: D. H. Werner, R. Mittra eds.), Frontiers in Electromagnetics, IEEE Press, 2000.

[12] F.L. Teixeira, W.C. Chew, "Systematic derivation of anisotropic PML absorbing media in cylindrical and spherical coordinates," IEEE Microwave Guided Wave Lett., Vol. 7, pp. 371–373, 1997.

[13] O. Ozgun, M. Kuzuoglu, "Non-Maxwellian locally-conformal PML absorbers for finite element mesh truncation," IEEE Trans. Antennas Propagat., Vol. 55, no. 3, pp. 931–937, 2007.

[14] O. Ozgun, M. Kuzuoglu, "Near-field performance analysis of locally-conformal perfectly matched absorbers via Monte Carlo simulations," J. Comput. Phys., Vol. 227, no. 2, pp. 1225–1245, 2007.

[15] O. Ozgun, M. Kuzuoglu, "Locally-conformal perfectly matched layer implementation for finite element mesh truncation," Microwave Opt. Technol. Lett., Vol. 48, no. 9, pp. 1836–1839, 2006.

[16] O. Ozgun, M. Kuzuoglu, "Locally-conformal and multi-center perfectly matched layer implementations for finite element mesh truncation," 2006 IEEE AP-S International Symposium and USNC/URSI National Radio Science Meeting, pp. 1753–1756, July 9–14 2006, Albuquerque, New Mexico, USA.

[17] O. Ozgun, M. Kuzuoglu, "Multi-center perfectly matched layer implementation for finite element mesh truncation," Microwave Opt. Technol. Lett., Vol. 49, no. 4, pp. 827–832, 2007.

[18] J.L. Volakis, A. Chatterjee, L.C. Kempel, Finite Element Method for Electromagnetics, IEEE Press, 1998.

[19] B.P. Sinha, R.H. MacPhie, "Electromagnetic scattering from prolate spheroids for axial incidence," IEEE Trans. Antennas Propagat., Vol. 23, no. 5, pp. 676–679, 1975.